Robust storage qubits in ultracold polar molecules

Philip D. Gregory[1], Jacob A. Blackmore[1], Sarah L. Bromley[1], Jeremy M. Hutson[2], and Simon L. Cornish[1*]
[1] *Joint Quantum Centre (JQC) Durham-Newcastle, Department of Physics, Durham University, Durham, United Kingdom, DH1 3LE.*
[2] *Joint Quantum Centre (JQC) Durham-Newcastle, Department of Chemistry, Durham University, Durham, United Kingdom, DH1 3LE.*

MOLECULAR CONSTANTS

The molecular constants used for the calculation of the rotational and hyperfine structure of ^{87}Rb^{133}Cs are given in Table I.

CROSSED OPTICAL DIPOLE TRAP APPARATUS

The light for the crossed optical dipole trap (xODT) is generated by a single-mode IPG fibre laser, with wavelength $\lambda = 1550$ nm. The two beams have waists of $81(1)\,\mu$m and $97(1)\,\mu$m and cross at an angle of 27°, with both beams propagating in the horizontal plane. There is a frequency difference of 100 MHz between the beams to avoid interference effects. Both beams are linearly polarised at an angle β with respect to the applied magnetic field, which is oriented along the vertical z direction. The angle β is set by manually rotating a $\lambda/2$ waveplate in each beam. For measurements with fixed xODT intensity of $15.8\,\mathrm{kW\,cm^{-2}}$ (Figs. 1 and 3), the trap frequencies experienced by the molecules in the rotational ground state are $(\omega_x, \omega_y, \omega_z)/2\pi = (29(1), 119(2), 116(2))$ Hz.

Molecules in different parts of the xODT experience different intensities, with a range determined by the ratio between the beam waist and the width of the molecule sample. The distribution of the molecules is Gaussian with standard deviations $\sigma = \sqrt{k_\mathrm{B}T/m\omega^2}$, where $T = 0.7\,\mu$K is the temperature of the molecules, such that $(\sigma_x, \sigma_y, \sigma_z) \approx (28, 6.9, 7.0)\,\mu$m. Due to gravitational sag, the centre of the distribution is $z_0 = g/\omega_z^2 \approx 18\,\mu$m below the position of peak intensity. Under these conditions, the variation of intensity across the cloud is dominated by the vertical direction and we estimate the 2σ intensity difference to be

$$\Delta I \approx \frac{8 z_0 \sigma_z}{w_0^2} I_\mathrm{pk} \approx 0.13 I_\mathrm{pk}, \tag{S1}$$

using the mean of the two beam waists, $\omega_0 = 89\,\mu$m. This represents an upper limit on the intensity variation that could contribute to decoherence in our experiments.

Constant	Value	Ref.
B_v	490.173 994(45) MHz	[1]
D_v	207.3(2) Hz	[2]
$(eQq)_\mathrm{Rb}$	−809.29(1.13) kHz	[1]
$(eQq)_\mathrm{Cs}$	59.98(1.86) kHz	[1]
c_Rb	29.4 Hz	[3]
c_Cs	196.8 Hz	[3]
c_3	192.4 Hz	[3]
c_4	19.019(105) kHz	[1]
g_r	0.0062	[3]
$g_\mathrm{Rb} \cdot (1 - \sigma_\mathrm{Rb})$	1.8295(24)	[1]
$g_\mathrm{Cs} \cdot (1 - \sigma_\mathrm{Cs})$	0.7331(12)	[1]

TABLE I. Constants involved in the molecular Hamiltonian for ^{87}Rb^{133}Cs. Terms without uncertainties are calculated using density-functional theory (DFT) [3]. Other terms are found by microwave spectroscopy of the rotational transitions [1, 2].

MICROWAVE APPARATUS

To drive the transition between $N = 0 \leftrightarrow 1$, we apply microwaves with a frequency of $2 \times B_v \approx 980$ MHz. The microwaves are generated using a pair of Keysight MXG N5183B signal generators, which are synchronised to a common 10 MHz GPS reference (Jackson Labs Fury). The outputs of both signal generators are connected to a single 3 W amplifier that drives a homebuilt antenna constructed from 1 mm diameter copper wire, cut to a length of $\lambda/4 \approx 7.7$ cm. The microwaves are polarised such that they drive both π and $\sigma^\pm$ transitions. Pulses are generated using the built-in pulse modulation mode on the signal generators which are controlled by transistor-transistor logic (TTL) signals derived from a field programmable gate array (FPGA) with microsecond timing resolution.

In experiments, we find that the resonant frequencies for the transitions depend linearly upon the intensity of the microwaves used to drive the transitions. This is due to off-resonant couplings to other nearby transitions between the rotational states. These energy shifts are $< h \times 3$ kHz for all measurements shown, and we have tested that the coherence times we measure do not depend upon the intensity of the microwaves used in the state preparation.

In Supp. Fig. 1 and Supp. Fig. 2 we show the available transitions for the two ground states used at 154.5 G $[(0,4)_1$ and $(0,3)_0]$ as well as the available transitions from the excited states $(1,4)_3$ and $(1,3)_2$ at a magnetic

field of 154.5 G. For a given sub-level of $N = 1$ there are fewer allowed transitions back to $N = 0$ due to the smaller total number of hyperfine sub-levels and so off-resonant coupling is less of a concern. We note that any $N = 1$ component which remains during the Ramsey hold will quickly dephase (coherence time less than 1 ms), and so if present would simply contribute a non-zero molecule number background to the Ramsey fringes. The absence of any non-zero background signal in Fig. 3 indicates that this is not an issue.

STATES AND TRANSITIONS USED IN THIS WORK

The molecular states that we label by $(N, M_F)_k$ in the main text are a superposition of the products of different molecular rotational states and nuclear spin states. To determine the coefficients of these states, we construct the Hamiltonian in the fully uncoupled basis with basis functions $|N, M_N, m_{\mathrm{Rb}}, m_{\mathrm{Cs}}\rangle$. The quantum number $M_F = M_N + m_{\mathrm{Rb}} + m_{\mathrm{Cs}}$ is conserved when the laser polarisation is parallel to the magnetic field ($\beta = 0$), but not otherwise. For each eigenstate, we calculate the expectation value $\langle\psi| F_z |\psi\rangle$ and label the state with the nearest integer value of M_F. We then order the states by energy to determine k. The composition of each of the states used in this work is shown in table II, with coefficients rounded to 1 part in 10^3. This rounding causes the table to omit coefficients that are non-zero and on the order of 1 part in 10^5 to 1 part in 10^6 for basis states with $N = 2$ in the ground rotational state. There are coefficients with a similar magnitude for basis states with $N = 3$ in the first rotationally excited state.

DERIVATION OF EQUATION 1 AND MAGNETIC FIELD LIMIT ON THE COHERENCE TIME AT $B = 154.52\,\mathrm{G}$

The coherence time T_2 is limited by variation ΔE_{01} in the energy difference between the two states such that

$$T_2 = \frac{h}{|\Delta E_{01}|}, \tag{S2}$$

where h is the Planck constant. The energy difference at a given magnetic field

$$E_{01}(B) = |E_{|0\rangle}(B) - E_{|1\rangle}(B)| \tag{S3}$$

can be calculated from the energies of the two states, $E_{|0\rangle}(B)$ and $E_{|1\rangle}(B)$. We plot E_{01} as a function of magnetic field in Supp. Fig. 3(a). The magnitude of ΔE_{01} is the difference between the maximum and minimum value of E_{01} experienced in a given measurement.

To explain the results shown in Fig. 1, we must evaluate E_{01} across the range of magnetic fields defined by the magnetic field noise ΔB. Away from the turning point at $B_0 = 154.52\,\mathrm{G}$, the minimum and maximum values of E_{01} are found at $B \pm \Delta B/2$. The variation in energy can therefore be evaluated by

$$\Delta E_{01} = |E_{01}(B + \Delta B/2) - E_{01}(B - \Delta B/2)|. \tag{S4}$$

At the turning point, the minimum and maximum values of E_{01} are found at B_0 and $B_0 \pm \Delta B/2$ respectively. The variation in energy here is

$$\Delta E_{01} = |E_{01}(B_0 \pm \Delta B/2) - E_{01}(B_0)|. \tag{S5}$$

The transition between these two regimes occurs when $|B - B_0| \approx \Delta B$.

Derivation of Equation 1

When the trap laser is polarised parallel to the magnetic field direction ($\beta = 0$), we find that the decoherence is dominated by the tensor light shifts across a wide range of magnetic fields around the turning point (see Supp. Fig. 4). As such we can reasonably approximate the magnetic field variation using just Eq. S4. To arrive at the fit function presented in Eq. 1, we calculate the Taylor expansion of Eq. S4 to find,

$$\Delta E_{01} = \frac{dE_{01}}{dB}(\Delta B) + \frac{1}{2}\frac{d^2E_{01}}{dB^2}(\Delta B)^2 + ... \tag{S6}$$

The first and second derivatives of energy with respect to magnetic field are plotted in Supp. Fig. 3(b) and (c), respectively. The second derivative of E_{01} is two orders of magnitude smaller than the first derivative at magnetic fields where the tensor light shifts do not dominate. For small variations in magnetic field $\Delta B < 1\,\mathrm{G}$, we can therefore approximate

$$\Delta E_{01} \approx \frac{dE_{01}}{dB}(\Delta B) \equiv \mu_{01}\Delta B, \tag{S7}$$

using only the first term in Eq. S6. Substituting Eq. S7 into Eq. S2 we find the coherence time limited by magnetic field noise

$$T_2' \approx \frac{h}{|\mu_{01}|\Delta B}. \tag{S8}$$

To include the differential tensor light shifts as an additional source of decoherence, with coherence time T_2^*, we combine the coherence times as

$$\frac{1}{T_2} = \frac{1}{T_2'} + \frac{1}{T_2^*}, \tag{S9}$$

to find the fit function

$$T_2 = \left(\frac{|\mu_{01}|\,\Delta B}{h} + \frac{1}{T_2^*}\right)^{-1}. \tag{S10}$$

Magnetic field limit on the coherence time at $B = 154.52\,\mathbf{G}$

We can estimate the limit placed on the coherence time by ΔB by at the turning point by performing a Taylor expansion of Eq. S5

$$\Delta E_{01} = \frac{dE_{01}}{dB}\left(\frac{\Delta B}{2}\right) + \frac{1}{2}\frac{d^2E_{01}}{dB^2}\left(\frac{\Delta B}{2}\right)^2 + ... \quad \text{(S11)}$$

At this magnetic field, $dE_{01}/dB = 0$, and so only the second derivative contributes. We calculate $d^2E_{01}/dB^2 = h \times 3.2\,\mathrm{Hz\,G^{-2}}$ (see Supp. Fig. 3(c)). For $\Delta B = 35\,\mathrm{mG}$, we therefore find

$$\Delta E_{01} = \frac{1}{2}\times(h\times 3.2)\times\left(\frac{0.035}{2}\right)^2 = h\times 0.49\,\mathrm{mHz}, \quad \text{(S12)}$$

with a corresponding coherence time of

$$T_2' = \frac{1}{0.49\,\mathrm{mHz}} = 2.0\times10^3\,\mathrm{s}. \quad \text{(S13)}$$

This is remarkably long and validates the omission of the second order term in Eq. S11 from the fit function in Eq. 1.

DERIVATION OF EQUATION 11

The function used to fit the observed Ramsey fringes is given in Eq. 11.

In the absence of decoherence and collisional loss of molecules from the trap, the Ramsey fringes are described by

$$N(T) = \frac{N_i}{2}\left[\cos(2\pi(\delta T + \phi)) + 1\right], \quad \text{(S14)}$$

where $N(T)$ is the number of molecules remaining in state $|0\rangle$, N_i is the total number of molecules, T is the hold time between the Ramsey pulses, and δ and ϕ are the frequency and phase of the Ramsey fringes. We include decoherence, with a characteristic $1/e$ coherence time T_2 as

$$N(T) = \frac{N_i}{2}\left[e^{-T/T_2}\cos(2\pi(\delta T + \phi)) + 1\right], \quad \text{(S15)}$$

where the addition of the exponential term reduces the contrast of the Ramsey fringes as T increases.

Collisional loss of molecules from the trap reduces the total number of molecules remaining in the sample, but does not affect the contrast of the fringes. We have previously shown that these losses are due to fast optical excitation of two-body collision complexes by the trap light [4], and the rate limiting step for this loss mechanism is therefore two-body [5]. Accordingly, the rate equation for the density of ground-state molecules $n(t)$ is

$$\frac{dn}{dt} = -K_2 n(t)^2, \quad \text{(S16)}$$

where K_2 is a two-body rate coefficient which characterises the loss with units $\mathrm{m^3\,s^{-1}}$. This equation can be rewritten in terms of the molecule number $N(t)$ by introducing an effective volume $V_{\mathrm{eff}} = (m\bar{\omega}/(4\pi k_{\mathrm{B}}T_{\mathrm{m}})^{-(3/2)}$ which depends on the temperature of the molecules T_{m} and the geometric mean of the trap frequencies $\bar{\omega} = (\omega_x\omega_y\omega_z)^{1/3}$. This yields

$$\frac{dN}{dt} = -\frac{K_2}{V_{\mathrm{eff}}}N(t)^2. \quad \text{(S17)}$$

To simplify the solution of this equation we assume that the temperature remains constant throughout the measurement. Rearranging and integrating then leads to

$$N(t) = \frac{N_i}{1 + \frac{K_2}{V_{\mathrm{eff}}}N_i t}, \quad \text{(S18)}$$

where N_i is the initial molecule number. To find the $1/e$ time which characterises this loss T_1 we must evaluate

$$N(T_1) = \frac{N_i}{1 + \frac{K_2}{V_{\mathrm{eff}}}N_i T_1} = \frac{N_i}{e}, \quad \text{(S19)}$$

which by rearrangement leads to

$$\frac{K_2}{V_{\mathrm{eff}}}N_i = \frac{e-1}{T_1}. \quad \text{(S20)}$$

Substituting Eq. S15 back into Eq. S13 yields

$$N(t) = \frac{N_i}{1 + \frac{t}{T_1}(e-1)}. \quad \text{(S21)}$$

To describe the Ramsey fringes in the presence of both decoherence and collisional loss, we must replace N_i in Eq. S10 with the expression for $N(t)$ in Eq. S16 to find the fit function given in Eq. 11 as a function of the Ramsey time T

$$N(T) = \frac{N_i}{2}\left(\frac{1}{1 + \frac{T}{T_1}[e-1]}\right) \times \left[e^{-T/T_2}\cos(2\pi(\delta T + \phi)) + 1\right]. \quad \text{(S22)}$$

It is worth noting that whilst T_1 is the time for the molecule number to fall to $1/e$ of the initial value, the decay is not exponential and so waiting $2T_1$ does not lead to the molecule number falling to $1/e^2$ of the initial value. This is an artefact of the density-dependent character of the two-body loss.

MATRIX ELEMENTS FOR H_{quad} AND H_{AC}

The dominant terms that contribute to the differential AC Stark shift between hyperfine states are H_{quad}

and H_{AC}. To be explicit, and to demonstrate the off-diagonality in N, we give the matrix elements for each of these terms here.

$$\begin{aligned}
&\langle N, M_N, m_{\mathrm{Rb}}, m_{\mathrm{Cs}}| H_{\mathrm{quad}} |N', M'_N, m'_{\mathrm{Rb}}, m'_{\mathrm{Cs}}\rangle = \\
&\sum_{M=-2}^{2} \Bigg\{ \sqrt{(2N+1)(2N'+1)}(-1)^M \\
&\times \begin{pmatrix} N & 2 & N' \\ -M_N & M & M'_N \end{pmatrix} \begin{pmatrix} N & 2 & N' \\ 0 & 0 & 0 \end{pmatrix} \\
&\times \Bigg[\left(\frac{(eqQ)_{\mathrm{Rb}}}{4} \right) (-1)^{M_N + I_{\mathrm{Rb}} - m_{\mathrm{Rb}}} \\
&\times \frac{\begin{pmatrix} I_{\mathrm{Rb}} & 2 & I_{\mathrm{Rb}} \\ -m_{\mathrm{Rb}} & -M & m'_{\mathrm{Rb}} \end{pmatrix}}{\begin{pmatrix} I_{\mathrm{Rb}} & 2 & I_{\mathrm{Rb}} \\ -I_{\mathrm{Rb}} & 0 & I_{\mathrm{Rb}} \end{pmatrix}} \delta_{m_{\mathrm{Cs}}, m'_{\mathrm{Cs}}} \\
&+ \left(\frac{(eqQ)_{\mathrm{Cs}}}{4} \right) (-1)^{M_N + I_{\mathrm{Cs}} - m_{\mathrm{Cs}}} \\
&\times \frac{\begin{pmatrix} I_{\mathrm{Cs}} & 2 & I_{\mathrm{Cs}} \\ -m_{\mathrm{Cs}} & -M & m'_{\mathrm{Cs}} \end{pmatrix}}{\begin{pmatrix} I_{\mathrm{Cs}} & 2 & I_{\mathrm{Cs}} \\ -I_{\mathrm{Cs}} & 0 & I_{\mathrm{Cs}} \end{pmatrix}} \delta_{m_{\mathrm{Rb}}, m'_{\mathrm{Rb}}} \Bigg] \Bigg\},
\end{aligned} \tag{S23}$$

In the above, terms in parentheses are Wigner-3j symbols, $\delta_{A,B}$ represents the Kronecker delta function and the coefficients have the same definition as in [1].

$$\begin{aligned}
&\langle N, M_N| H_{\mathrm{AC}} |N', M'_N\rangle = -\frac{I\alpha^{(0)}}{2\epsilon_0 c} \delta_{N,N'} \delta_{M_N, M'_N} \\
&-\frac{I\alpha^{(2)}}{2\epsilon_0 c} \sum_M d^2_{M0}(\beta) (-1)^{M'_N} \sqrt{(2N+1)(2N'+1)} \\
&\times \begin{pmatrix} N' & 2 & N \\ 0 & 0 & 0 \end{pmatrix} \begin{pmatrix} N' & 2 & N \\ -M'_N & M & M_N \end{pmatrix}.
\end{aligned} \tag{S24}$$

Here, I is the laser intensity, $\delta_{A,B}$ is a Kronecker delta and $d^2_{M0}(\beta)$ is a reduced Wigner rotation matrix. The term proportional to the isotropic part, $\alpha^{(0)}$, produces an equal energy shift of all (N, M_N). The term proportional to the anisotropic part, $\alpha^{(2)}$, has more complicated behavior: for $N > 0$ it has elements both diagonal and off-diagonal in N, M_N that depend on β.

VALIDATING THE FORM OF EQUATION 4

Our model for the rotational and hyperfine structure of RbCs is able to replicate the structure of the AC Stark shift observed in experiments, and is used to calculate the magnetic field dependencies presented in Fig. 1 and Fig. 2(d). However, for Fig. 2(c) and (e) a simplified fit function is used, given by Eq. 2 and Eq. 3, and we use our full Hamiltonian to calculate the numerical factor $X(B)$. The simpler fit function was then used to find the optimal value for the anisotropic polarisability $\alpha^{(2)}$ and the free-space detuning δ_0. In Supp. Fig. 5 we show the calculations using the full Hamiltonian for all of the results in Fig. 2(c)-(e). We see that our full model is well described by the simpler fit function we use in the main text.

ADDITIONAL SYSTEMATIC UNCERTAINTIES IN THE MEASUREMENT OF $\alpha^{(2)}$

There are additional systematic contributions to the uncertainty in $\alpha^{(2)}$. Uncertainty in I contributes additional uncertainty of $\pm 2\,\%$ to $\alpha^{(2)}$. There is also uncertainty from the compositions of the states which is more difficult to quantify due to the large number of parameters in the Hamiltonian. The largest contribution to the mixing of N is from the Rb electric quadrupole coupling, characterised by the constant $(eQq)_{\mathrm{Rb}}$; the uncertainty from this parameter contributes an uncertainty in $\alpha^{(2)}$ of $\pm 1\,\%$. The fitted value of $\alpha^{(2)}$ lies intermediate between the two values we previously obtained from microwave spectra on the $N = 0 \leftrightarrow 1$ transitions [6].

VARIATION OF THE AC STARK EFFECT WITH MAGNETIC FIELD

The differential AC Stark shift is highly dependent on the nuclear spin state of the molecules. In the experiment we investigate only a small range of magnetic fields. Here we present the full calculation as a function of magnetic field from 0 to 1000 G.

To determine this behaviour we extract the eigenvalues of the Hamiltonian as a function of the strength of the applied magnetic field for zero intensity. Each continuous energy level is labelled by M_F which is determined by the expectation value $\langle\psi| F_z |\psi\rangle$ for each eigenstate $|\psi\rangle$. We repeat this analysis for a second intensity $I = 60\ \mathrm{kW\,cm^{-2}}$ with $\beta = 0°$. As the differential AC Stark shift we are investigating is linear, we extract the differential polarisability by determining the slope of the change of the energy difference between the two states as a function of intensity.

In Supp. Fig. 6 we show this gradient as a function of the applied magnetic field. As the magnetic field increases the gradient of the AC Stark shift eventually reaches some asymptotic value. This occurs because there are multiple competing terms in the total Hamiltonian that mix both rotational and nuclear spin states. However the Zeeman effect acts mostly on the nuclear spin states, which ultimately causes the nuclear spin states to decouple such that the overall molecular wavefunction is best represented by the product of a single rotational state $|N, M_N\rangle$ and nuclear spin state $|m_{\mathrm{Rb}}, m_{\mathrm{Cs}}\rangle$. At high magnetic field $|0\rangle$ and $|2\rangle$ differ by 1 in the value

of m_{Rb} and by 2 in the value of m_{Cs}; as the dominant off-diagonal term is the Rb nuclear electric quadrupole coupling, we believe that it is the difference in Rb nuclear spin projection that contributes to the large differential effective polarisability.

ESTIMATING THE MINIMUM COHERENCE TIME IN FIG. 4

Our Ramsey measurements yield oscillations in the number of molecules remaining in $|0\rangle$ as a function of time. For the results in Figs. 1 and 2, we fit the oscillations using the model shown in Eq. 11. Fitting is performed by a least-squares regression. T_2^* cannot be determined from the results shown in Fig. 3, because the sum of squares of residuals decreases continuously as $T_2 \to \infty$, as shown in Supp. Fig. 7(a).

To estimate the minimum value of T_2^* which is consistent with our results in Fig. 3, we replace the fit parameter with a coherence rate coefficient $\beta = 1/T_2$ such that the fit function becomes,

$$N(T) = N_i \left(\frac{1}{1 + \frac{T}{T_1} \times [e-1]} \right) \times \frac{1}{2} \times \left[e^{-\beta T} \cos(\delta T + \phi) + 1 \right]. \tag{S25}$$

As $T_2 \to \infty$, $\beta \to 0$, and we find a minimum in the residual sum of squared as shown in Supp. Fig. 7(b). We find an optimum value of $\beta = -0.026\,\mathrm{s}^{-1}$ with root mean square (RMS) deviation $\sigma = 0.103\,\mathrm{s}^{-1}$.

In the main text we report a 90 % confidence interval for the minimum value of T_2^*, which we find using the methods laid out by Feldman and Cousins [7]; this approach unifies the treatment of one- and two-sided confidence intervals. We apply the method to a model with Gaussian statistics

$$P(\beta|\beta_{\mathrm{true}}) = \frac{1}{\sigma\sqrt{2\pi}} \exp\left(-\frac{(\beta - \beta_{\mathrm{true}})^2}{2\sigma^2} \right), \tag{S26}$$

where β is the measured value of β_{true}, the true value of the parameter, with RMS deviation σ. We consider the case where $\beta_{\mathrm{true}} > 0$; this is valid for our experiments as a negative value of β is non-physical, corresponding to increasing coherence over the experiment. The 90 % confidence intervals are shown in Supp. Fig. 8, which we calculate using the same procedure as described in [8]. The vertical line at $\beta/\sigma \approx -0.026/0.103 \approx -0.251$ indicates our measured value, which puts a corresponding 90 % upper limit on $\beta_{\mathrm{true}} \approx 1.41\sigma \approx 0.145\,\mathrm{s}^{-1}$. This upper limit on β corresponds to a lower limit on $T_2^* = 1/\beta_{\mathrm{true}} = 6.9\,\mathrm{s}$ (90 % confidence level).

CONFIRMING THE ABSENCE OF COLLISIONAL SHIFTS

To look for evidence of collisional energy shifts we separate the results shown in Fig. 3 into six time-intervals, each 204 ms long. We then fit the Ramsey fringes in each time-interval independently and plot the result in Supp. Fig. 9(a). Over the 1200 ms we interrogate the sample, the number of molecules remaining drops to $0.23N_i$. We estimate that two-body loss will increase the temperature of the sample from $0.7\,\mu$K to $\sim 1.0\,\mu$K over this time. The density n of the sample therefore reduces by the fraction

$$\frac{n}{n_{\mathrm{i}}} = \frac{N}{N_{\mathrm{i}}} \left(\frac{T}{T_{\mathrm{i}}} \right)^{-3/2} \approx 0.23 \times \left(\frac{1.0}{0.7} \right)^{-3/2} = 0.13, \tag{S27}$$

where n_{i} is the starting density of the sample. We see no significant change in the detuning of the microwaves as the density of the sample reduces, as shown in Supp. Fig. 9(b) where we plot the results as a function of the molecular density.

* s.l.cornish@durham.ac.uk

[1] P. D. Gregory, J. Aldegunde, J. M. Hutson, and S. L. Cornish, Controlling the rotational and hyperfine state of ultracold ^{87}Rb^{133}Cs molecules, Phys. Rev. A **94**, 041403(R) (2016).

[2] J. A. Blackmore, P. D. Gregory, S. L. Bromley, and S. L. Cornish, Coherent manipulation of the internal state of ultracold ^{87}Rb^{133}Cs molecules with multiple microwave fields, Phys. Chem. Chem. Phys. 10.1039/d0cp04651e (2020).

[3] J. Aldegunde, B. A. Rivington, P. S. uchowski, and J. M. Hutson, Hyperfine energy levels of alkali-metal dimers: Ground-state polar molecules in electric and magnetic fields, Phys. Rev. A **78**, 033434 (2008).

[4] P. D. Gregory, J. A. Blackmore, S. L. Bromley, and S. L. Cornish, Loss of ultracold ^{87}Rb^{133}Cs molecules via optical excitation of long-lived two-body collision complexes, Phys. Rev. Lett. **124**, 163402 (2020).

[5] P. D. Gregory, M. D. Frye, J. A. Blackmore, E. M. Bridge, R. Sawant, J. M. Hutson, and S. L. Cornish, Sticky collisions of ultracold RbCs molecules, Nat. Comms **10**, 3104 (2019).

[6] P. D. Gregory, J. A. Blackmore, J. Aldegunde, J. M. Hutson, and S. L. Cornish, ac stark effect in ultracold polar ^{87}Rb^{133}Cs molecules, Phys. Rev. A **96**, 021402(R) (2017).

[7] G. J. Feldman and R. D. Cousins, Unified approach to the classical statistical analysis of small signals, Physical Review D **57**, 3873 (1998).

[8] J. Baron, W. C. Campbell, D. DeMille, J. M. Doyle, G. Gabrielse, Y. V. Gurevich, P. W. Hess, N. R. Hutzler, E. Kirilov, I. Kozyryev, B. R. O'Leary, C. D. Panda, M. F. Parsons, B. Spaun, A. C. Vutha, A. D. West, E. P. West, and ACME Collaboration, Methods, analysis, and the treatment of systematic errors for the electron electric dipole moment search in thorium monoxide, New J. Phys. **19**, 073029 (2017).

$B\,(G)$	$\|0\rangle$	$\|1\rangle$	$\|2\rangle$	E_{02}/h (kHz)	E_{12}/h (kHz)
110.1	$(0,4)_1 \equiv$ $-0.487\,\|0,0,3/2,5/2\rangle$ $-0.874\,\|0,0,1/2,7/2\rangle$	$(0,3)_0 \equiv$ $0.833\,\|0,0,3/2,3/2\rangle$ $-0.522\,\|0,0,1/2,5/2\rangle$ $+0.183\,\|0,0,-1/2,7/2\rangle$	$(1,3)_2 \equiv$ $0.054\,\|1,1,3/2,1/2\rangle$ $-.059\,\|1,1,1/2,3/2\rangle$ $-0.294\,\|1,1,-0.5,5/2\rangle$ $-0.318\,\|1,1,-3/2,7/2\rangle$ $+0.272\,\|1,0,3/2,3/2\rangle$ $+0.199\,\|1,0,1/2,5/2\rangle$ $-0.169\,\|1,0,-1/2,7/2\rangle$ $+0.523\,\|1,-1,3/2,5/2\rangle$ $+0.625\,\|1,-1,1/2,7/2\rangle$	980,246.295	980,327.278
145.2	$(0,4)_1 \equiv$ $0.39\,\|0,0,3/2,5/2\rangle$ $+0.920\,\|0,0,1/2,7/2\rangle$	$(0,3)_0 \equiv$ $-0.893\,\|0,0,3/2,3/2\rangle$ $+0.435\,\|0,0,1/2,5/2\rangle$ $-0.113\,\|0,0,-1/2,7/2\rangle$	$(1,3)_2 \equiv$ $-0.036\,\|1,1,3/2,1/2\rangle$ $+0.0287\,\|1,1,1/2,3/2\rangle$ $+0.205\,\|1,1,-1/2,5/2\rangle$ $+0.290\,\|1,1,-1.5,7/2\rangle$ $-0.195\,\|1,0,3/2,3/2\rangle$ $-0.171\,\|1,0,1/2,5/2\rangle$ $+0.129\,\|1,0,-1/2,7/2\rangle$ $-0.467\,\|1,-1,3/2,5/2\rangle$ $+0.755\,\|1,-1,1/2,7/2\rangle$	980,259.464	980,336.593
154.5	$(0,4)_1 \equiv$ $0.372\,\|0,0,3/2,5/2\rangle$ $+0.928\,\|0,0,1/2,7/2\rangle$	$(0,3)_0 \equiv$ $0.905\,\|0,0,3/2,3/2\rangle$ $+0.415\,\|0,0,1/2,5/2\rangle$ $+0.100\,\|0,0,-1/2,7/2\rangle$	$(1,3)_2 \equiv$ $-0.032\,\|1,1,3/2,1/2\rangle$ $+0.023\,\|1,1,1/2,3/2\rangle$ $+0.186\,\|1,1,-1/2,5/2\rangle$ $+0.281\,\|1,1,-3/2,7/2\rangle$ $-0.179\,\|1,0,3/2,3/2\rangle$ $-0.162\,\|1,0,1/2,5/2\rangle$ $+0.120\,\|1,0,-1/2,7/2\rangle$ $-0.450\,\|1,-1,3/2,5/2\rangle$ $-0.781\,\|1,-1,1/2,7/2\rangle$	980,262.071	980,339.056
181.6	$(0,4)_1 \equiv$ $0.321\,\|0,0,3/2,5/2\rangle$ $0.947\,\|0,0,1/2,7/2\rangle$	$(0,3)_0 \equiv$ $0.928\,\|0,0,3/2,3/2\rangle$ $-0.365\,\|0,0,1/2,5/2\rangle$ $-0.074\,\|0,0,1/2,7/2\rangle$	$(1,3)_1 \equiv$ $-0.080\,\|1,1,3/2,1/2\rangle$ $+0.219\,\|1,1,1/2,3/2\rangle$ $+0.162\,\|1,1,-1/2,5/2\rangle$ $-0.110\,\|1,1,-3/2,7/2\rangle$ $-0.687\,\|1,0,3/2,3/2\rangle$ $-0.045\,\|1,0,1/2,5/2\rangle$ $-0.018\,\|1,0,-1/,7/2\rangle$ $-0.540\,\|1,-1,3/2,5/2\rangle$ $+0.375\,\|1,-1,1/2,7/2\rangle$	980,182.991	980,260.992
217.4	$(0,4)_1 \equiv$ $-0.269\,\|0,0,3/2,5/2\rangle$ $-0.963\,\|0,0,1/2,7/2\rangle$	$(0,3)_0 \equiv$ $0.949\,\|0,0,3/2,3/2\rangle$ $-0.312\,\|0,0,1/2,5/2\rangle$ $+0.051\,\|0,0,1/2,7/2\rangle$	$(1,4)_3 \equiv$ $-0.323\,\|1,1,3/2,3/2\rangle$ $-0.585\,\|1,1,1/2,5/2\rangle$ $+0.355\,\|1,1,-1/2,7/2\rangle$ $-0.092\,\|1,0,3/2,5/2\rangle$ $+0.645\,\|1,0,1/2,7/2\rangle$ $-0.048\,\|1,-1,3/2,7/2\rangle$	980,427.082	980,508.760
154.5	$(0,4)_1 \equiv$ $0.372\,\|0,0,3/2,5/2\rangle$ $+0.928\,\|0,0,1/2,7/2\rangle$	$(0,3)_0 \equiv$ $0.904\,\|0,0,3/2,3/2\rangle$ $-0.415\,\|0,0,1/2,5/2\rangle$ $+0.100\,\|0,0,-1/2,7/2\rangle$	$(1,4)_3 \equiv$ $0.478\,\|1,1,3/2,3/2\rangle$ $+0.517\,\|1,1,1/2,5/2\rangle$ $-0.455\,\|1,1,-1/2,7/2\rangle$ $+0.109\,\|1,0,3/2,5/2\rangle$ $-0.529\,\|1,0,1/2,7/2\rangle$ $-0.067\,\|1,-1,3/2,7/2\rangle$	980,399.341	980,476.326

TABLE II. Compositions of states used in this work, written in the uncoupled basis $|N, M_N, m_{\mathrm{Rb}}, m_{\mathrm{Cs}}\rangle$ with coefficients rounded to one part in 10^3. At each magnetic field, $|1\rangle$ is chosen to couple well to both $|0\rangle$ and $|2\rangle$. For the measurement at 154.5 G presented in Fig. 1, $|1\rangle = (1,3)_2$. This state has very weak coupling on the $|1\rangle \leftrightarrow |2\rangle$ transition. The measurements in Fig. 2 and Fig. 3, are also at 154.5 G but instead use $|1\rangle = (1,4)_3$, which has significantly better coupling on this transition, but requires the use of the more complicated pulse sequence shown inset in Fig. 3. The final two columns give the calculated transition frequencies in free space.

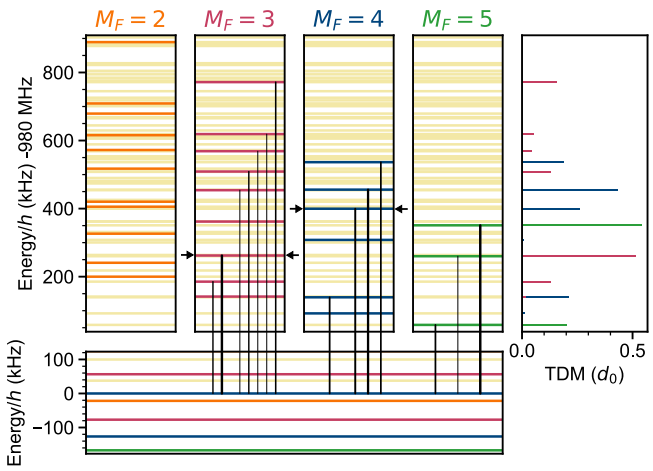

(a) $(0,4)_1 \leftrightarrow (1, M_F)$

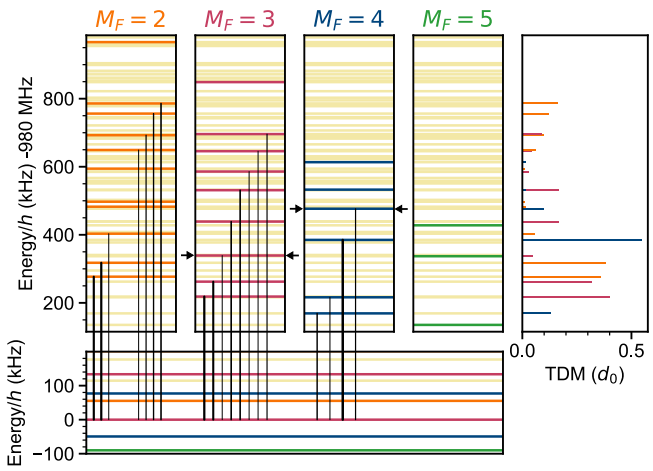

(b) $(0,3)_0 \leftrightarrow (1, M_F)$

Supp. Fig. 1. Transitions from the hyperfine states $(0,4)_1$ and $(0,3)_0$ of the $N = 0$ rotational state to $N = 1$ at 154.5 G. Each state is coloured by the value of M_F, allowed transitions have $M_F \to M_F - 1, M_F, M_F + 1$ with a strength described by the transition dipole moment (TDM) here shown in units of the permanent dipole moment of the molecule $d_0 \approx 1.23$ D. The vertical lines connect the labelled initial state for (a) and (b) to excited states via the electric dipole allowed transitions, the thickness of the line corresponds to the strength of the transition. For both (a) and (b) the initial state is labelled as the zero of energy. The target states used in this work are indicated by the arrows.

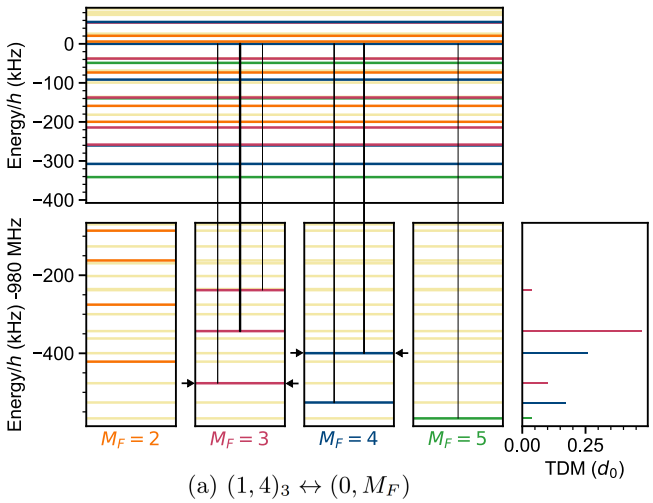

(a) $(1,4)_3 \leftrightarrow (0, M_F)$

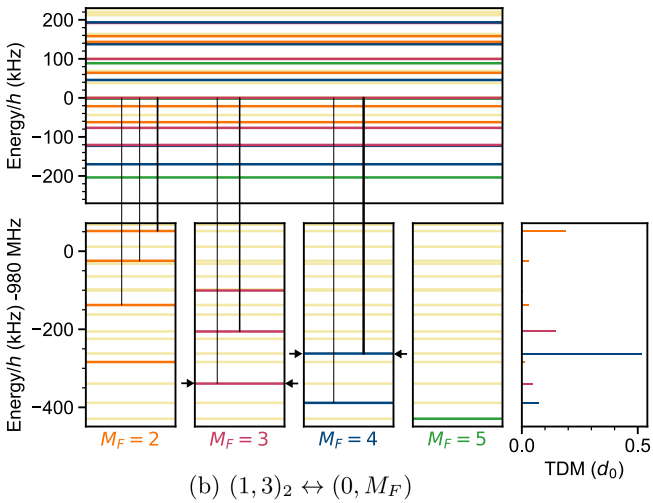

(b) $(1,3)_2 \leftrightarrow (0, M_F)$

Supp. Fig. 2. Transitions from the hyperfine states $(1,4)_3$ and $(1,3)_2$ of the $N = 1$ rotational state to $N = 0$ at 154.5 G. Each state is coloured by the value of M_F, allowed transitions have $M_F \to M_F - 1, M_F, M_F + 1$ with a strength described by the transition dipole moment (TDM) here shown in units of the permanent dipole moment of the molecule $d_0 \approx 1.23$ D. The vertical lines connect the labelled initial state for (a) and (b) to the hyperfine sub-levels of the ground state via the electric dipole allowed transitions, the thickness of the line corresponds to the strength of the transition. For both (a) and (b) the initial state is labelled as the zero of energy. The target states used in this work are indicated by the arrows.

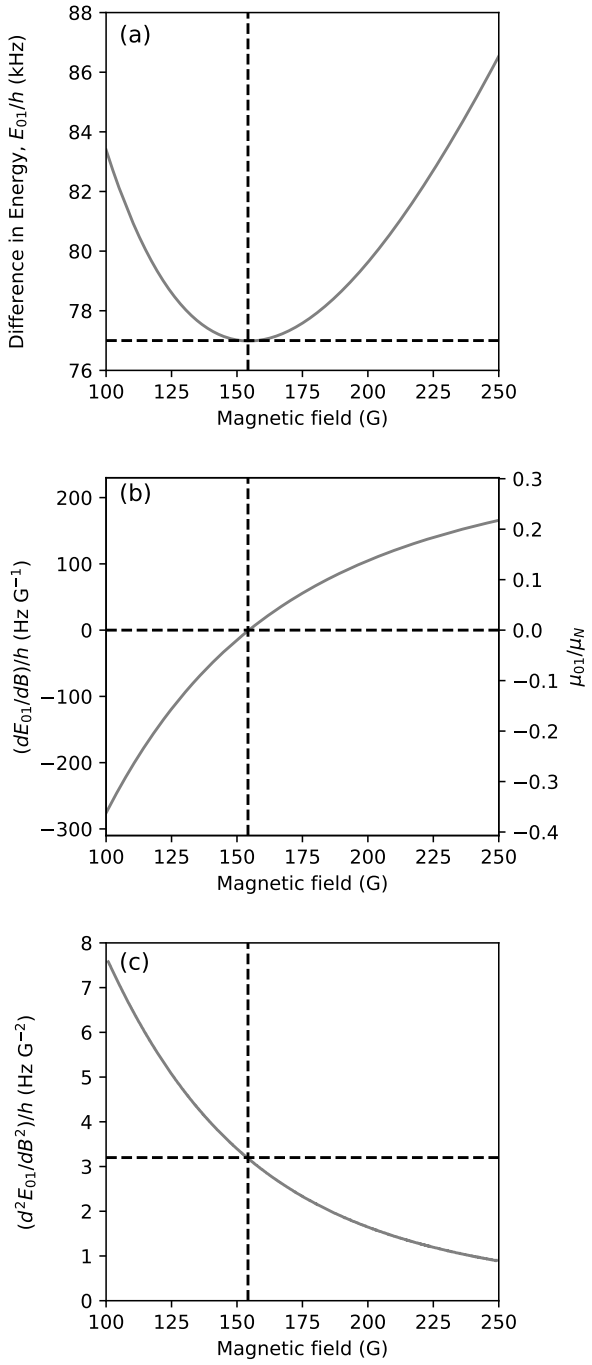

Supp. Fig. 3. (a) Differential Zeeman shift between the states $E_{01} = |E_{|0\rangle} - E_{|1\rangle}|$ along with the (b) first and (c) second derivatives of E_{01} with respect to magnetic field. The first derivative $dE_{01}/dB = \mu_{01} = 0$ at a magnetic field of $B = 154.52\,\mathrm{G}$ indicating a turning point in E_{01}.

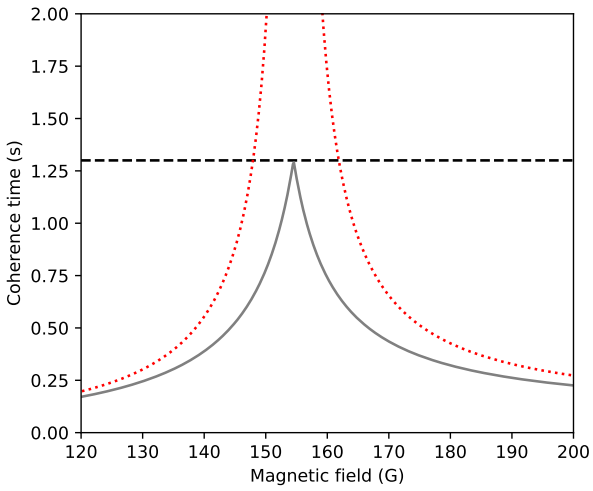

Supp. Fig. 4. Coherence time calculated for $\Delta B = 35\,\mathrm{mG}$. The red dotted line indicates the expected coherence time for magnetic field noise alone, calculated using the expression in Eq. S8. The gray solid line is the complete model including decoherence from the tensor light shifts ($T_2^* = 1.3\,\mathrm{s}$) that is present when the trap laser is polarised parallel to the magnetic field direction ($\beta = 0$), as presented in the main text. The horizontal dashed line indicates the coherence time limited by the tensor light shifts alone, which dominates the coherence time for magnetic fields across a broad range of magnetic fields around the turning point.

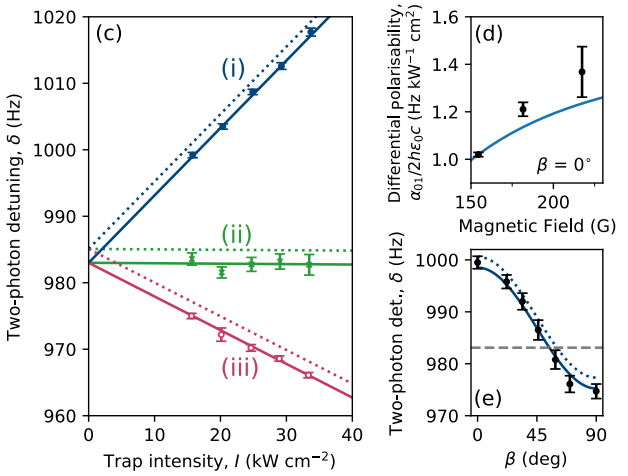

Supp. Fig. 5. Differential tensor light shifts from the full rotation and hyperfine calculation. Here we have reproduced the experimental results shown in Fig. 2(c)-(e), together with the results of the simple fit function given by Eq.(3) and Eq.(4). In addition, the dotted lines indicate the output of the full rotation and hyperfine calculation, including the difference in the free-space detuning highlighted in the main text. The solid lines have the free-space detuning fixed to be $\delta_0 = 983.0\,\mathrm{Hz}$. We see that the intensity dependence is nearly identical to the simpler model presented in Fig. 2(c) and (e), which indicates that our simpler equations capture the behaviour of the differential tensor light shifts well.

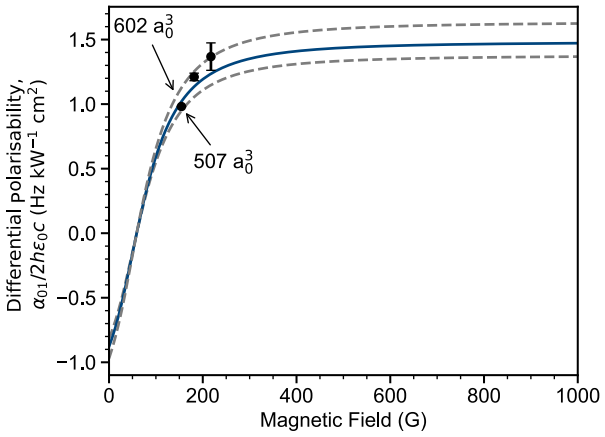

Supp. Fig. 6. The gradient of the differential AC Stark shift as a function of the applied magnetic field. The data points and the solid blue line are the same as in Fig. 2(d). The gray dashed lines correspond to the two values of $\alpha^{(2)}$ reported in [6] and are labelled by $\alpha^{(2)}/4\pi\epsilon_0$.

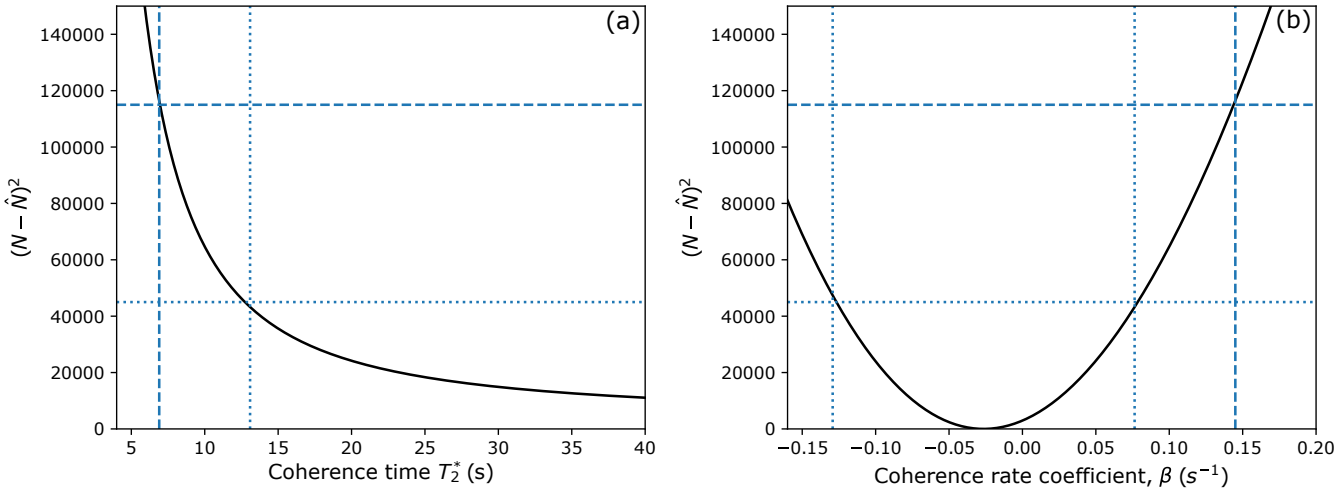

Supp. Fig. 7. Change in the residual sum of squares as a function of the free parameters (a) T_2^* and (b) $\beta = 1/T_2^*$ when fitting the results presented in Fig. 3. The minimum value of the residuals is 8604837, found at the minima seen in (b). This value is subtracted from the y-axes of both sets of data to give the change in residuals from this minimum value. The dotted lines indicate $\pm 1\sigma$ from the mean value found in (b). The dashed lines indicate the 90 % confidence interval for the minimum value of the coherence time T_2 consistent with our results.

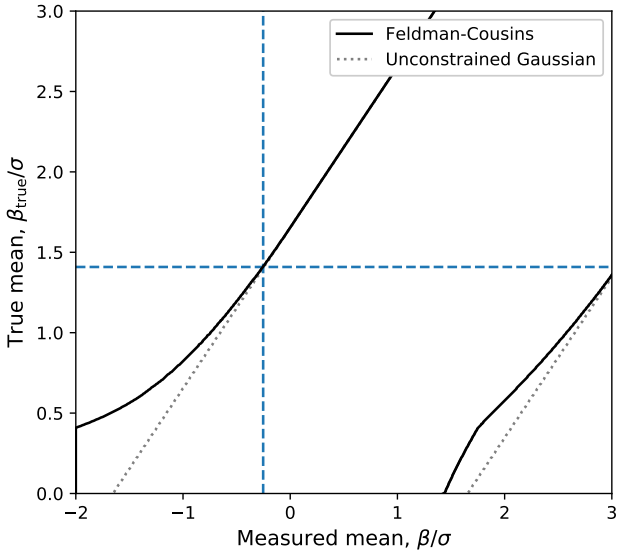

Supp. Fig. 8. The 90 % confidence bands for the mean of a Gaussian distribution which is constrained to be non-negative using the Feldman-Cousins approach (solid lines). The 90 % confidence bands for an unconstrained Gaussian distribution are also shown (dotted lines). The dashed vertical lines indicate the measured value of $\beta/\sigma = -0.251$. The dashed horizontal line shows where the vertical line intersects the 90 % upper boundary when $\beta_{\text{true}} \approx 1.41\sigma$.

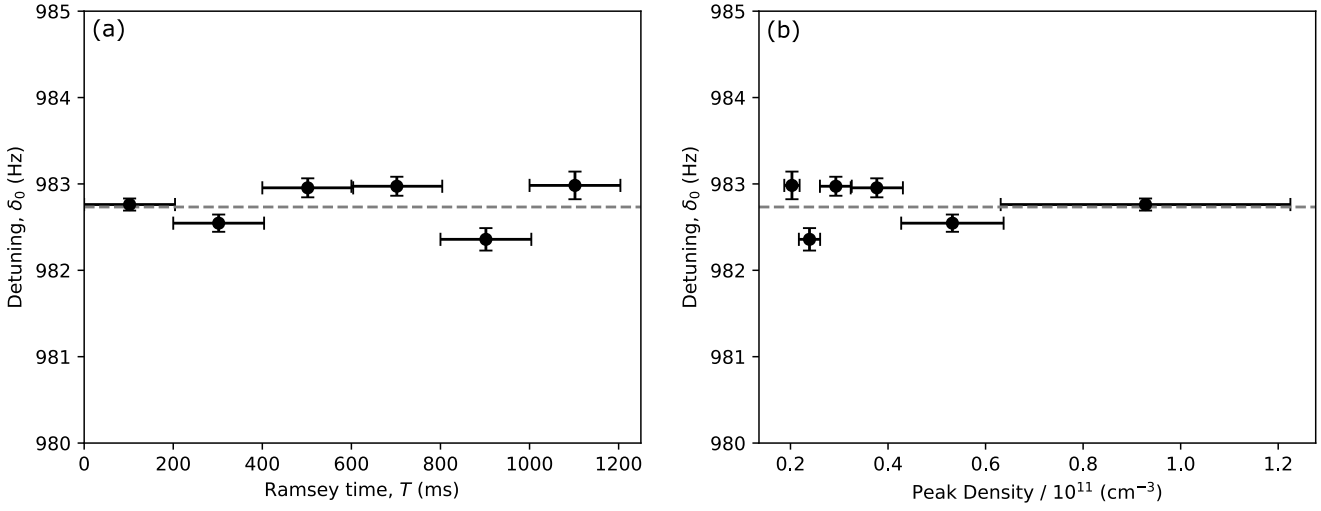

Supp. Fig. 9. Detuning measured from the Ramsey fringes presented in Fig. 3, but segmented into shorter 204 ms time intervals. As the Ramsey time increases, the density of the sample reduces due to two-body loss of molecules from the trap. We plot the detuning as a function of **(a)** time and **(b)** peak density. Each interval is indicated by the x error bars, with the marker indicating the centre of the interval. The dashed horizontal line is the detuning found when fitting across the whole dataset. We see no evidence that the detuning is dependent upon the density.